Supplementary Information (SI) for Inorganic Chemistry Frontiers.
This journal is © the Partner Organisations 2025

SUPPORTING INFORMATION

Highly optically diluted lanthanide coordination polymers with unexpected strong luminescence.

Chloé Blais,[a] Aurélien Chang,[a] Christine Hénaff,[a] Carole Daiguebonne,[a] * Aimin Yao,[a] Régis Gautier,[a] Guillaume Calvez,[a] Yan Suffren,[a] Kevin Bernot,[a] and Olivier Guillou[a,b] *.

[a] Univ Rennes, INSA Rennes, ENSCR, CNRS UMR 6226 "Institut des Sciences Chimiques de Rennes", 35708 Rennes, France.

[b] Institut Universitaire de France, 1 rue Descartes, 75005 Paris, France

* To whom correspondence should be addressed.

Olivier.guillou@insa-rennes.fr

Carole.Daiguebonne@insa-rennes.fr

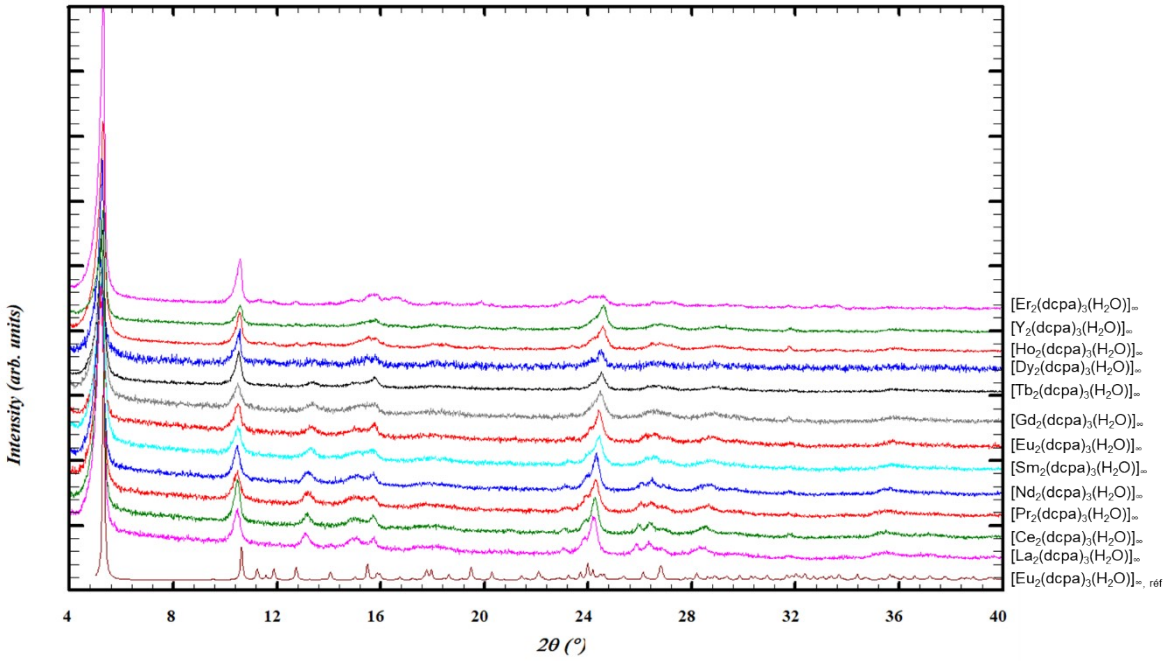

Figure S1. Experimental X-ray powder diffraction diagrams of $[Ln_2(dcpa)_3(H_2O)]_\infty$ with Ln = La-Er except Pm plus Y and simulated powder diffraction pattern of $[Eu_2(dcpa)_3(H_2O)]_\infty$ from its crystal structure (CCDC-1551529).

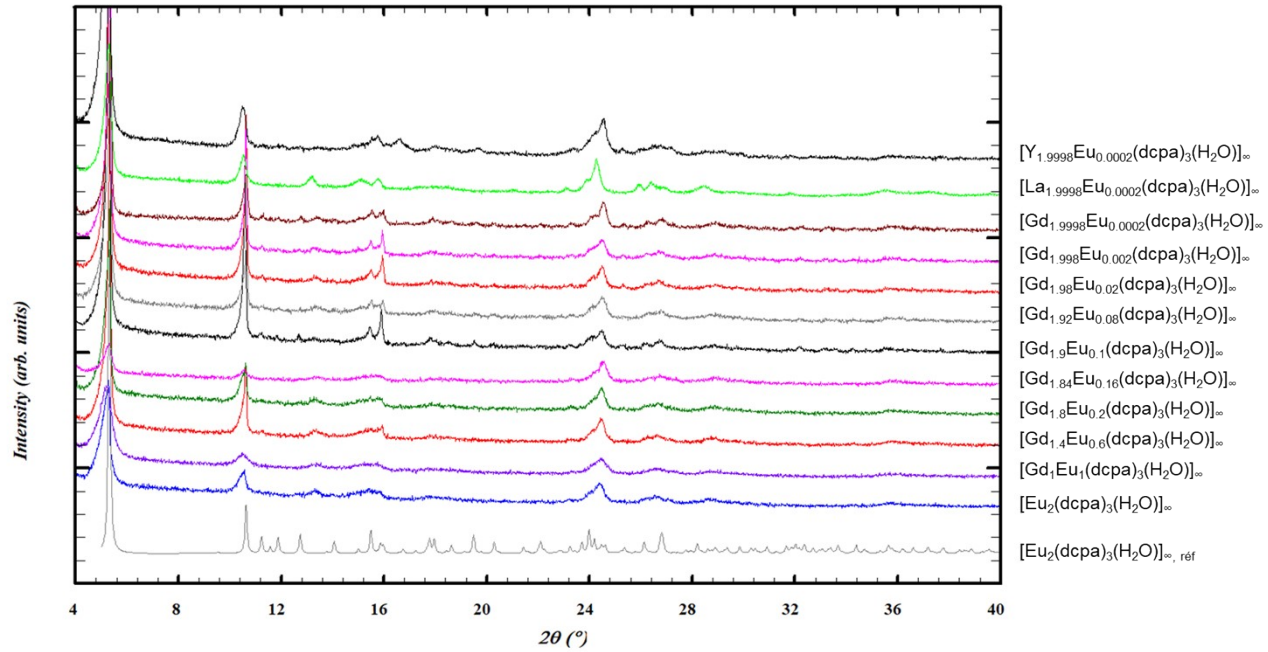

Figure S2. Experimental X-ray powder diffraction diagrams of $[Gd_{2-2x}Eu_{2x}(dcpa)_3(H_2O)]_\infty$ with $0.0001 \leq x \leq 1$, $[La_{2-2x}Eu_{2x}(dcpa)_3(H_2O)]_\infty$ and $[Y_{2-2x}Eu_{2x}(dcpa)_3(H_2O)]_\infty$ with $x = 0.0001$ and simulated powder diffraction pattern of $[Eu_2(dcpa)_3(H_2O)]_\infty$ from its crystal structure (CCDC-1551529).

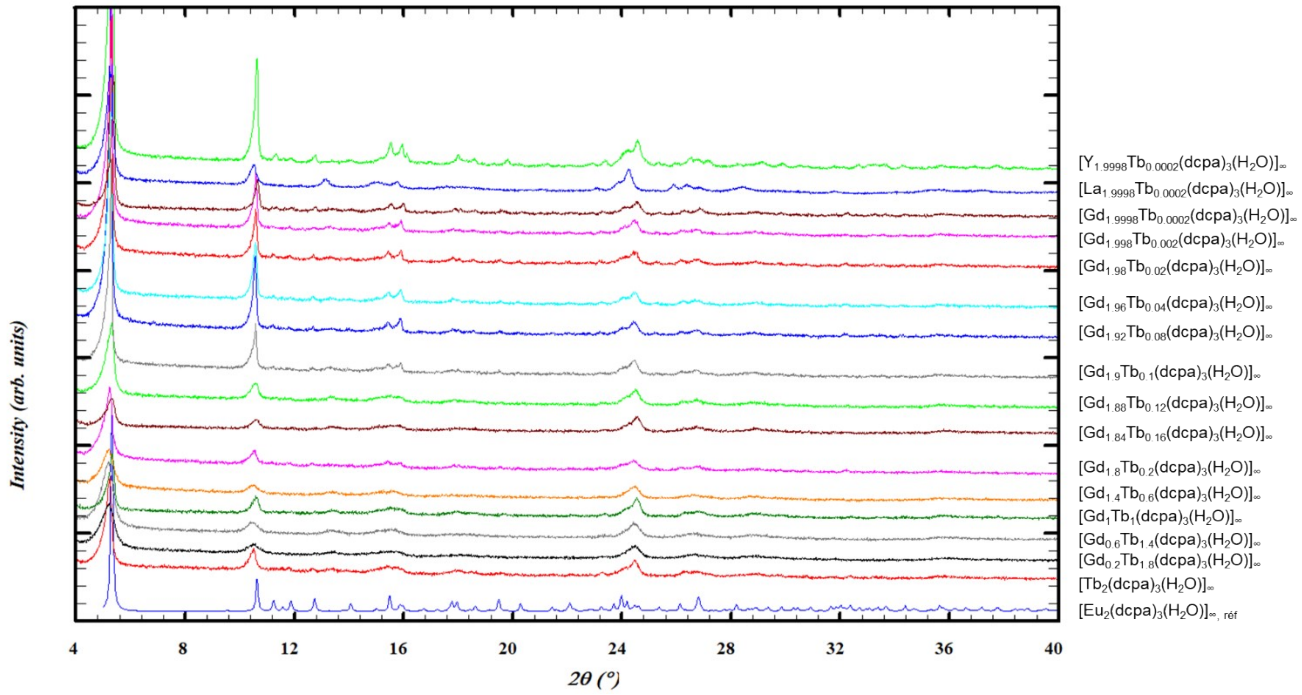

Figure S3. Experimental X-ray powder diffraction diagrams of $[Gd_{2-2x}Tb_{2x}(dcpa)_3(H_2O)]_\infty$ with $0.0001 \leq x \leq 1$, $[La_{2-2x}Tb_{2x}(dcpa)_3(H_2O)]_\infty$ and $[Y_{2-2x}Tb_{2x}(dcpa)_3(H_2O)]_\infty$ with $x = 0.0001$ and simulated powder diffraction pattern of $[Eu_2(dcpa)_3(H_2O)]_\infty$ from its crystal structure (CCDC-1551529).

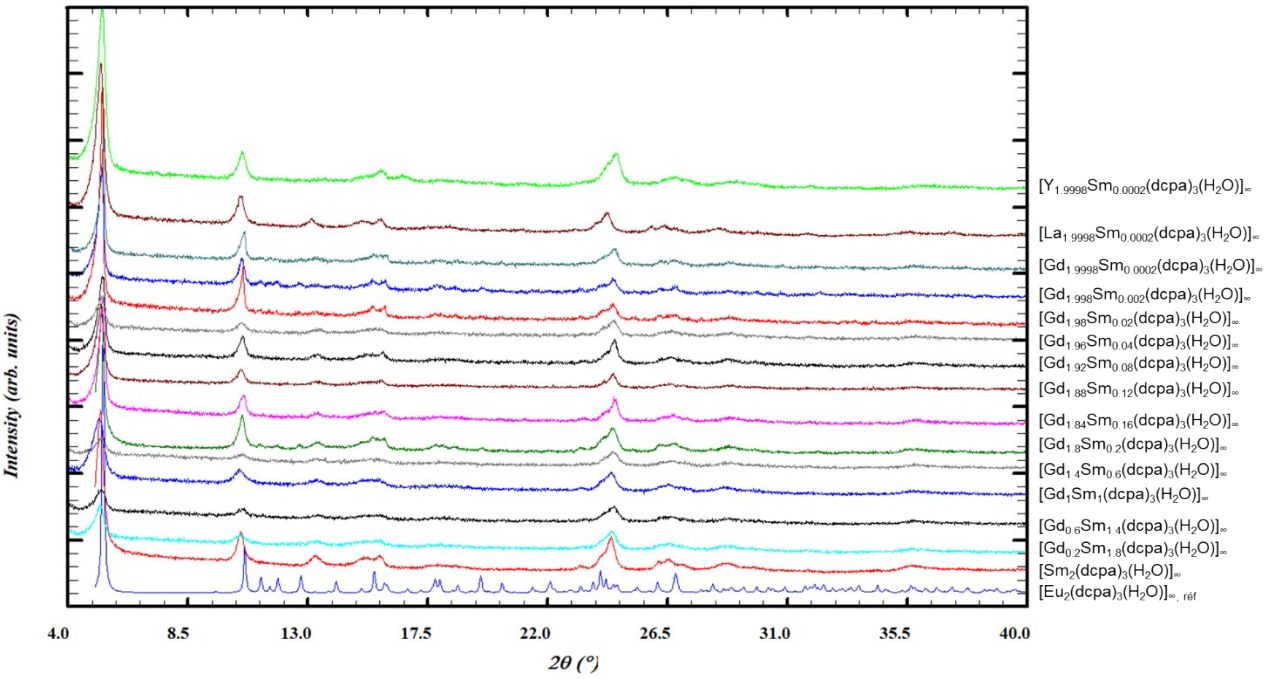

Figure S4. Experimental X-ray powder diffraction diagrams of $[Gd_{2-2x}Sm_{2x}(dcpa)_3(H_2O)]_\infty$ with $0.0001 \leq x \leq 1$, $[La_{2-2x}Sm_{2x}(dcpa)_3(H_2O)]_\infty$ and $[Y_{2-2x}Sm_{2x}(dcpa)_3(H_2O)]_\infty$ with $x = 0.0001$ and simulated powder diffraction pattern of $[Eu_2(dcpa)_3(H_2O)]_\infty$ from its crystal structure (CCDC-1551529).

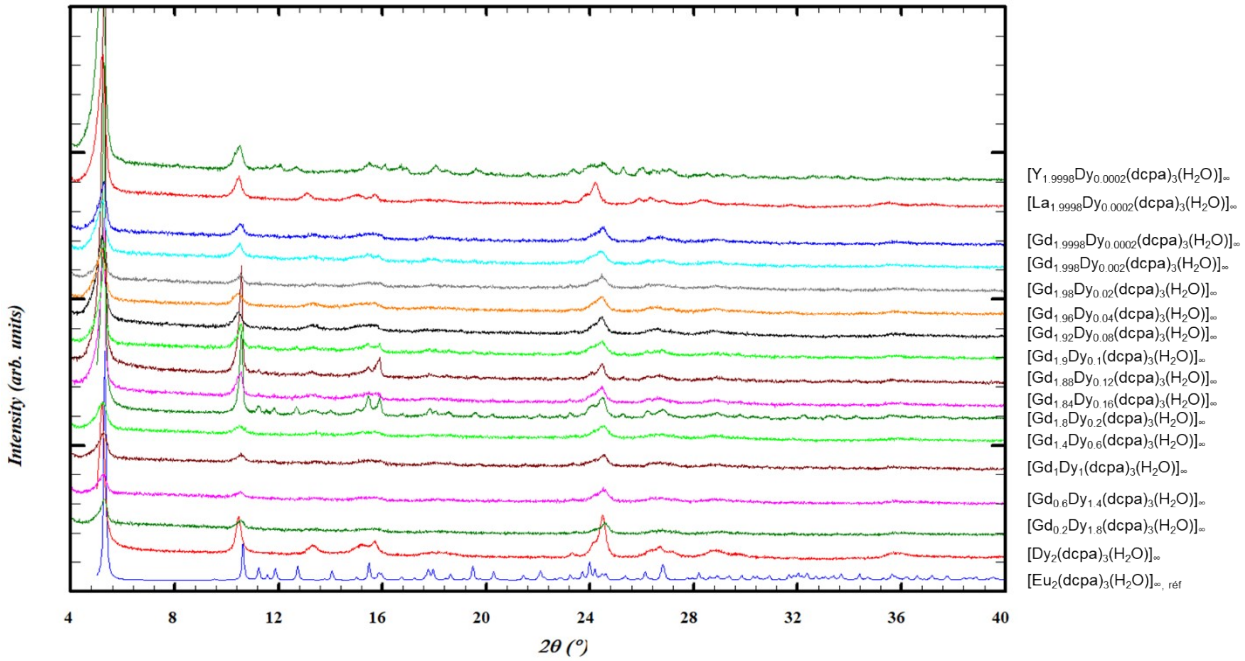

Figure S5. Experimental X-ray powder diffraction diagrams of $[Gd_{2-2x}Dy_{2x}(dcpa)_3(H_2O)]_\infty$ with $0.0001 \leq x \leq 1$, $[La_{2-2x}Dy_{2x}(dcpa)_3(H_2O)]_\infty$ and $[Y_{2-2x}Dy_{2x}(dcpa)_3(H_2O)]_\infty$ with $x = 0.0001$ and simulated powder diffraction pattern of $[Eu_2(dcpa)_3(H_2O)]_\infty$ from its crystal structure (CCDC-1551529).

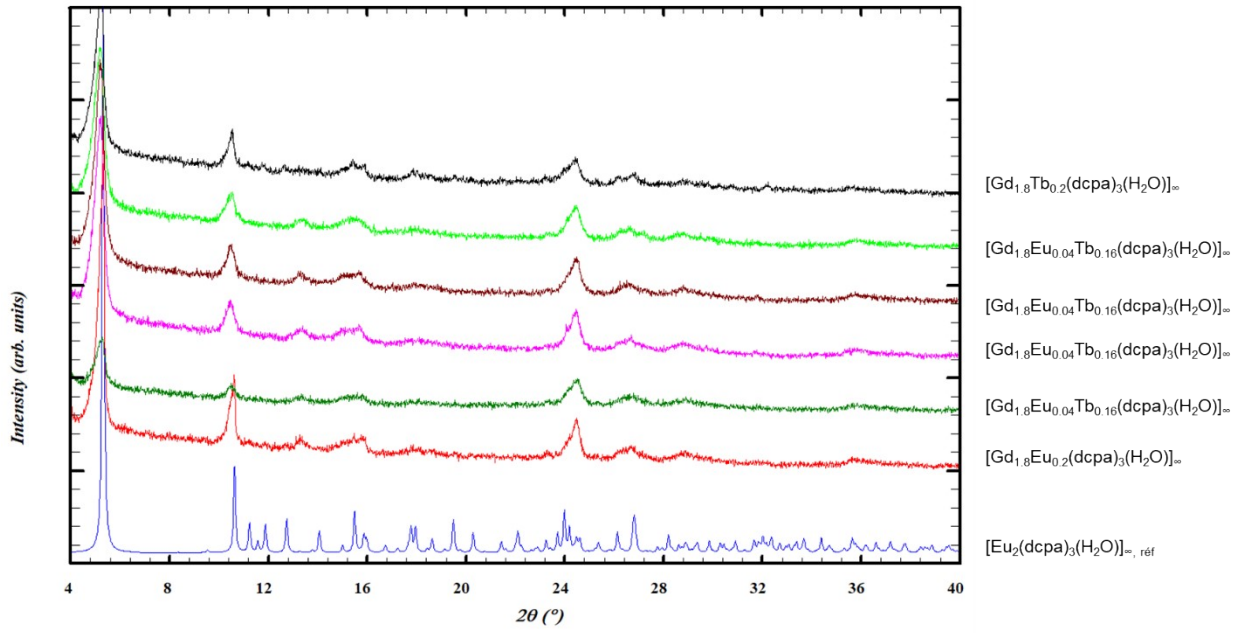

Figure S6. Experimental X-ray powder diffraction diagrams of $[Gd_{1.8}Eu_{0.2-0.2x}Tb_{0.2x}(dcpa)_3(H_2O)]_\infty$ with $0 \leq x \leq 1$ and simulated powder diffraction pattern of $[Eu_2(dcpa)_3(H_2O)]_\infty$ from its crystal structure (CCDC-1551529).

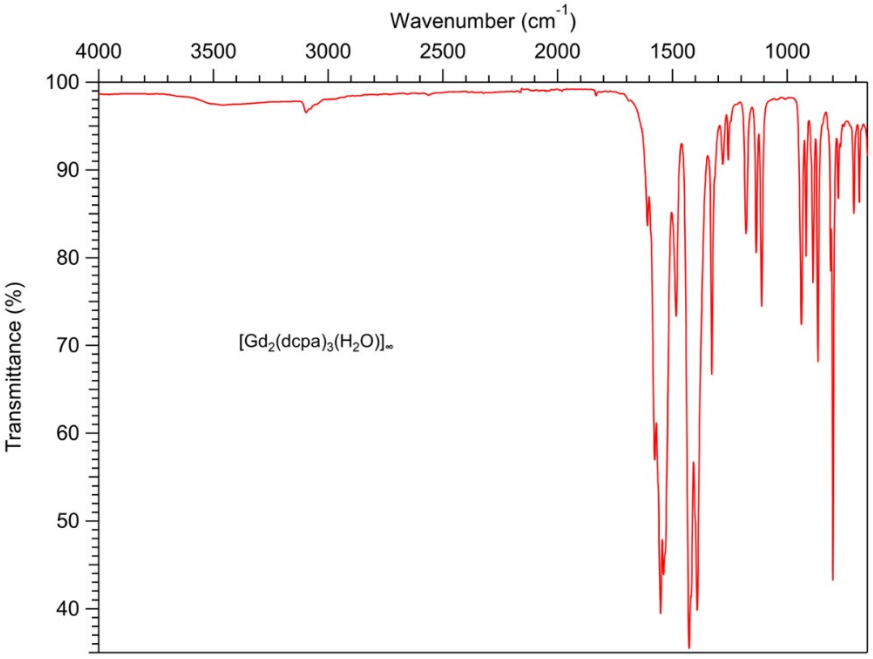

Figure S7. Solid state IR spectrum of $[Gd_2(dcpa)_3(H_2O)]_\infty$.

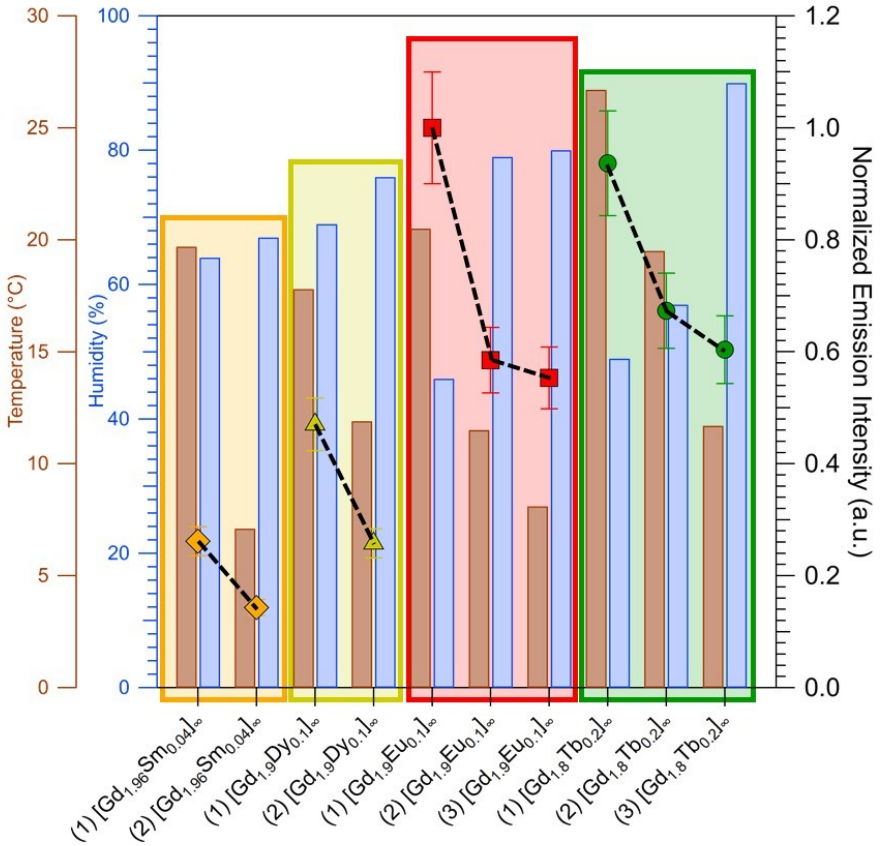

Figure S8. Luminescence intensities of $[Gd_{1.96}Sm_{0.04}(dcpa)_3(H_2O)]_\infty$, $[Gd_{1.9}Dy_{0.1}(dcpa)_3(H_2O)]_\infty$, $[Gd_{1.80}Eu_{0.2}(dcpa)_3(H_2O)]_\infty$ and $[Gd_{1.8}Tb_{0.2}(dcpa)_3(H_2O)]_\infty$, *versus* climatic conditions during the preparation of the microcrystalline powders. The numbers (1), (2) and (3) refer to different samples.

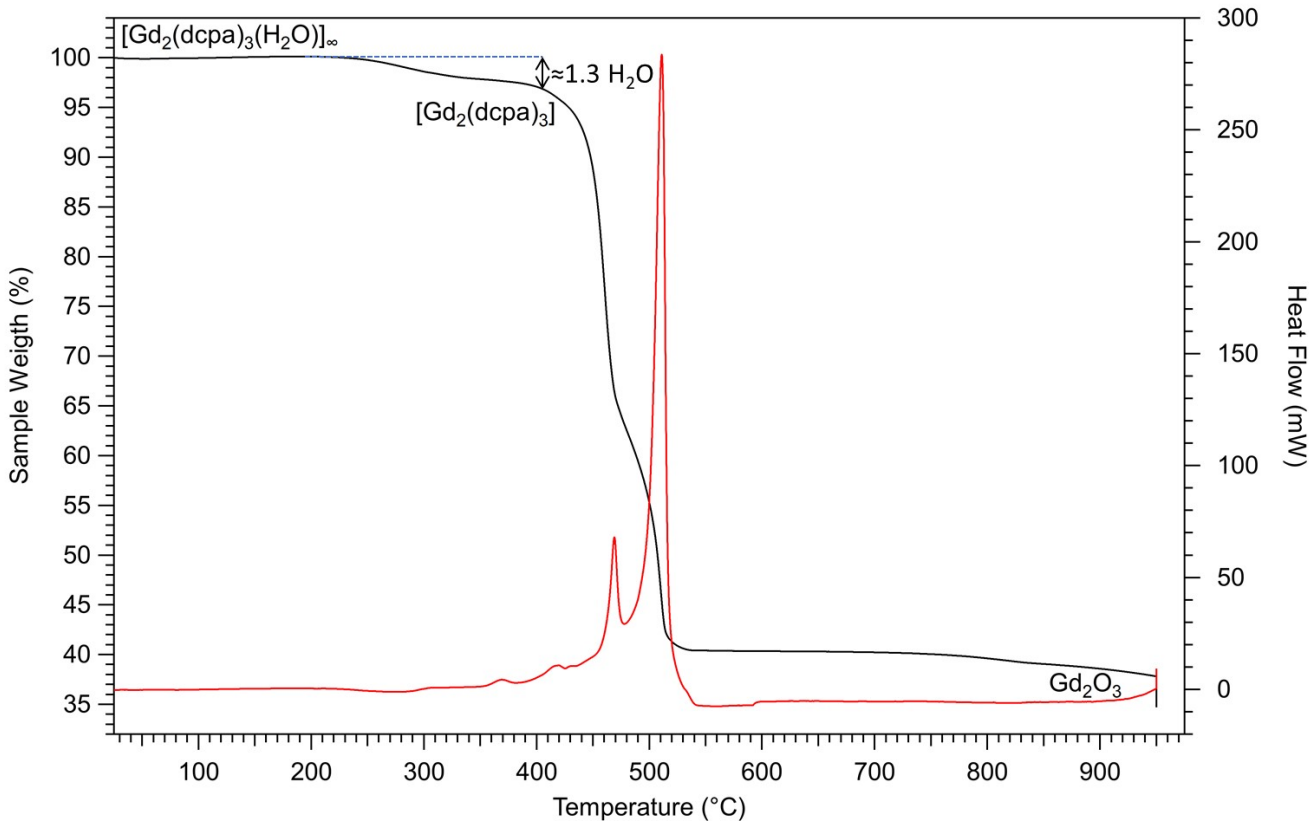

Figure S9. Thermal analysis of $[Gd_2(dcpa)_3(H_2O)]_\infty$ under air flux in a platinum crucible.

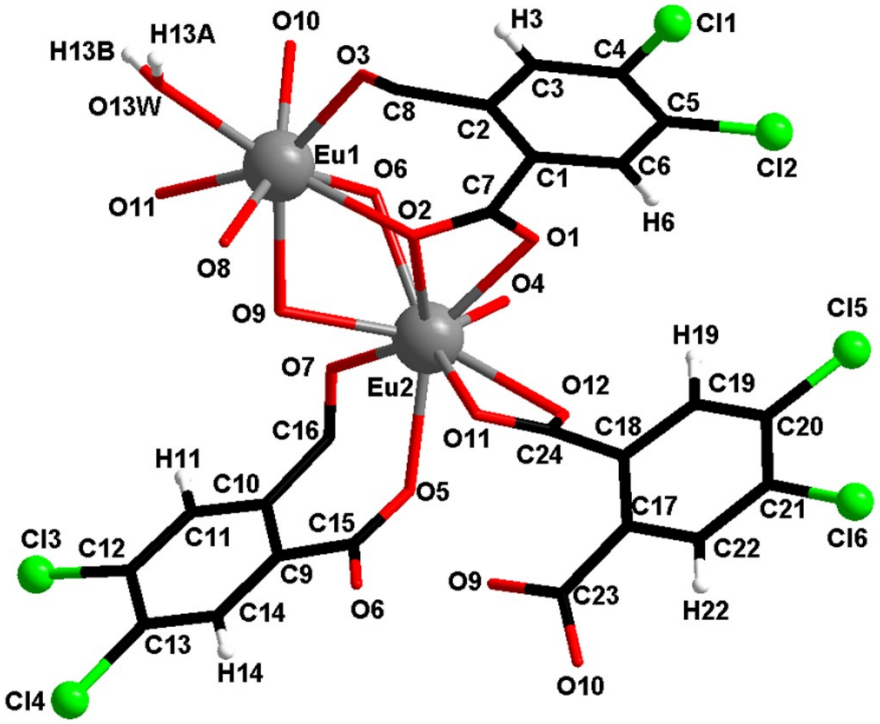

Figure S10. Projection view of an extended asymmetric unit of $[Eu_2(dcpa)_3(H_2O)]_\infty$ with the numbering scheme.

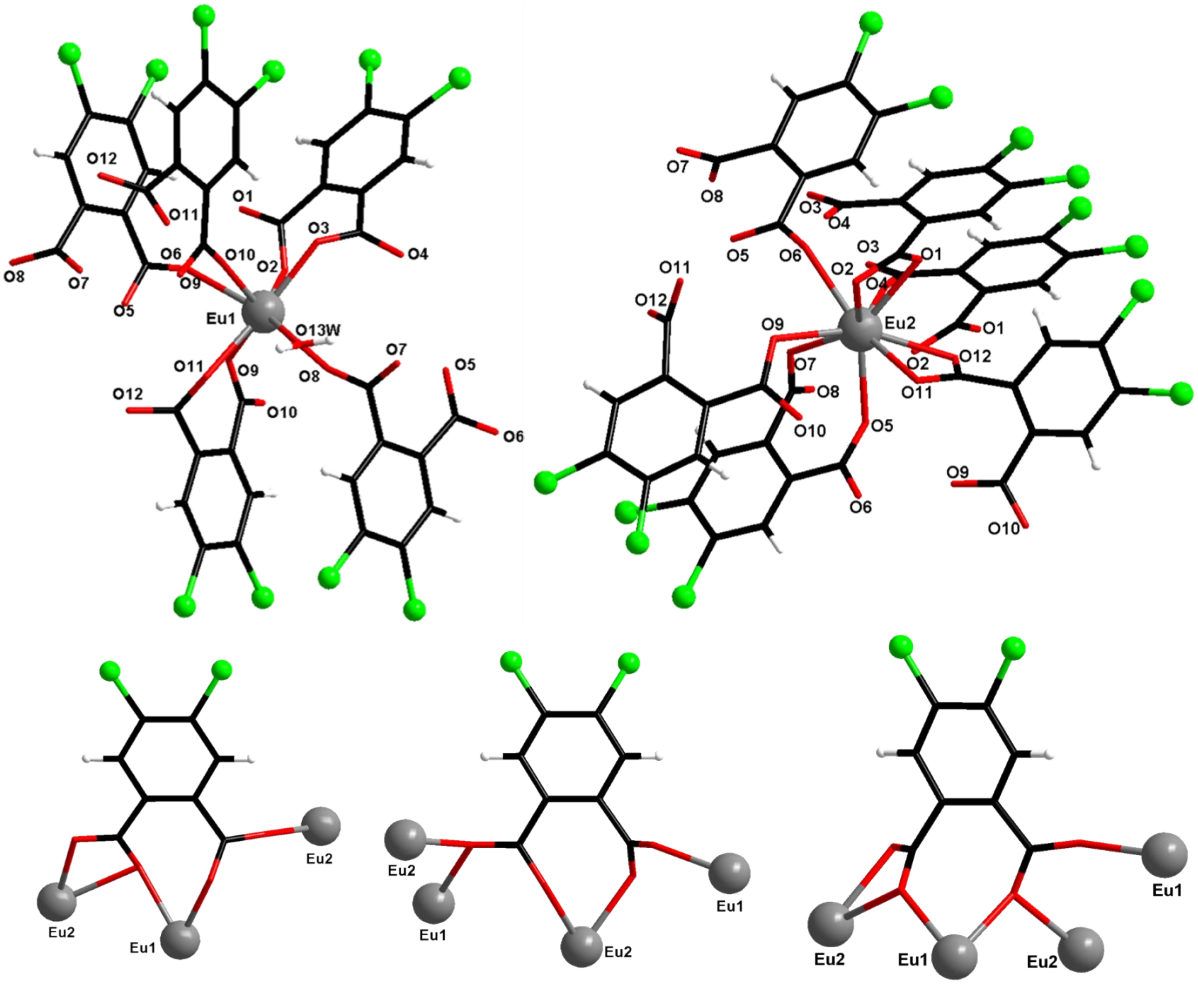

Figure S11. Lanthanide ions environments (top) and coordination modes of the $dcpa^{2-}$ ligands (bottom) in $[Eu_2(dcpa)_3(H_2O)]_\infty$.

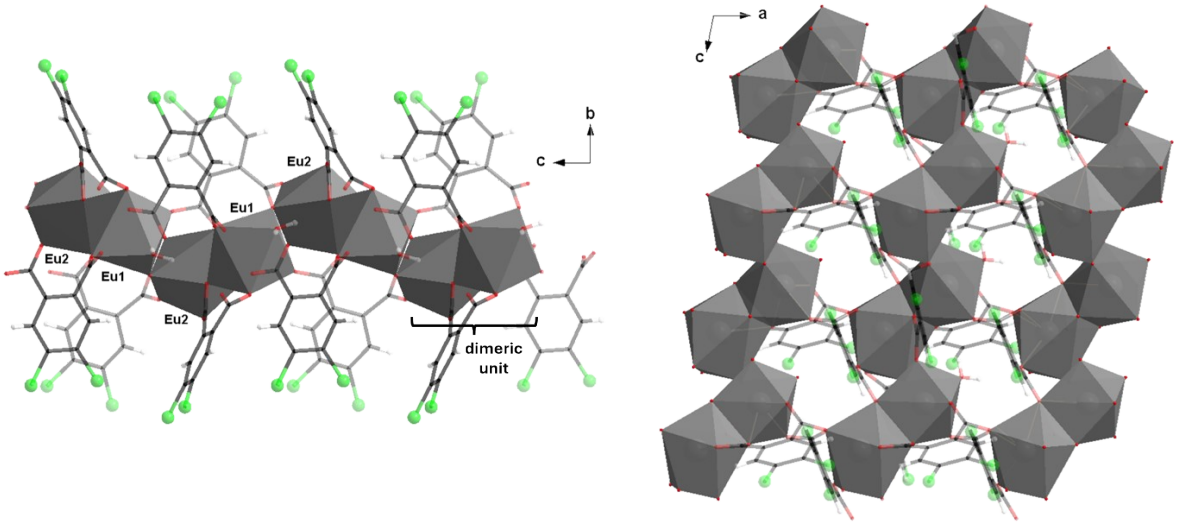

Figure S12. Projection views along the *a*- and *b*-axis of a chain-like molecular motif (left) and of a bidimensional molecular motif (right) of $[Eu_2(dcpa)_3(H_2O)]_\infty$.

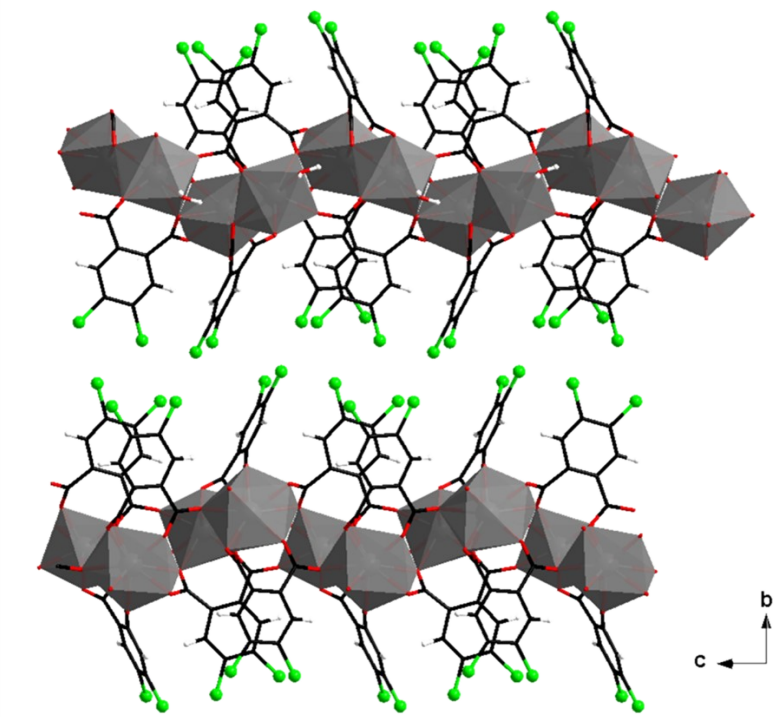

Figure S13. Projection view along the *a*-axis of two adjacent molecular planes of $[Eu_2(dcpa)_3(H_2O)]_\infty$.

Table S1. Mean distance between emissive lanthanide ions *versus* the doping rate in molecular alloys of general chemical formula $[Ln_{2x}Ln'_{2-2x}(dcpa)_3(H_2O)]_\infty$.

Doping rate of emissive ions (%)	Mean distance between emissive lanthanide ions (Å)
0.01	95.2
0.1	44.2
0.5	25.5
1	20.5
2	17.3
4	13.6
5	11.4
6	10.5
8	9.5
10	8.9
20	6.0
30	5.5
40	4.8
50	4.2
60	4.1
70	4.0
80	3.9
90	3.9
100	3.8

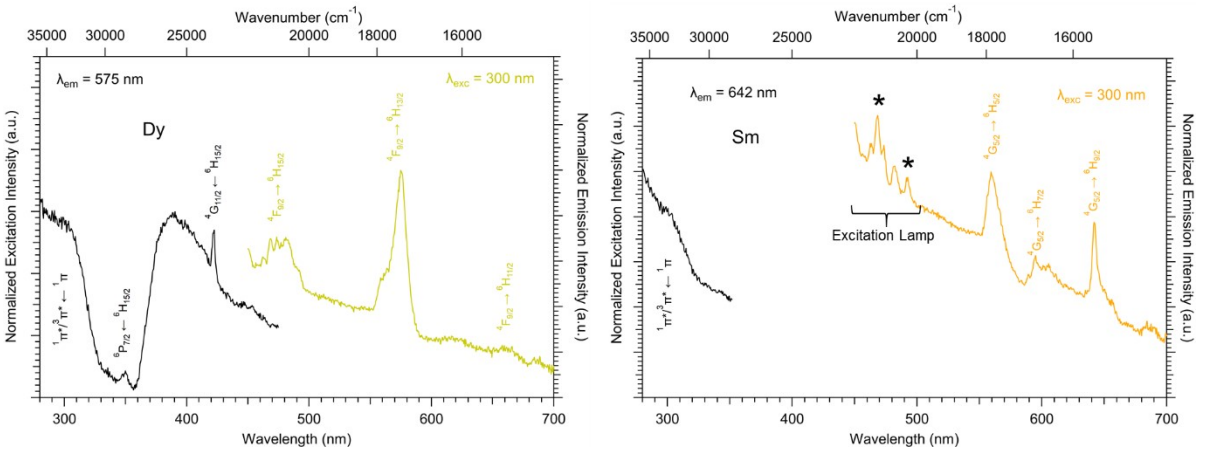

Figure S14. Room temperature solid-state excitation and emission spectra of $[Ln_2(dcpa)_3(H_2O)]_\infty$ with Ln = Dy (left) and Sm (right). Stars indicate emission peaks due to the excitation lamp.

Table S2. O-O distances in $[Eu_2(dcpa)_3(H_2O)]_\infty$.

Atom1	Atom2	Symmetry	Distance (Å)
O13W	O11	x, y, z	2.8396(34)
	O8	1+x, 1/2-y, 1/2+z	2.8759(33)
	O7	1+x, 1/2-y, 1/2+z	2.9153(29)
	O5	1+x, y, z	2.9767(35)
	O2	x, 1/2-y, -1/2+z	2.9904(30)
	O10	x, 1/2-y, -1/2+z	3.0104(33)
	O8	1+x, y, z	3.0885(33)
	O3	x, y, z	3.2396(35)

Table S3. Cl-Cl distances in $[Eu_2(dcpa)_3(H_2O)]_\infty$.

Atom1	Atom2	Symmetry	Distance (Å)
Cl1	Cl2	x, y, z	3.1765(15)
Cl2	Cl1	x, y, z	3.1765(15)
	Cl6	2-x, -1/2+y, 3/2-z	3.3464(14)
	Cl4	1-x, -y, 1-z	3.4222(15)
Cl3	Cl4	x, y, z	3.1867(13)
Cl4	Cl3	x, y, z	3.1866(13)
	Cl5	1-x, -1/2+y, 1/2-z	3.3280(14)
	Cl2	1-x, -y, 1-z	3.4218(15)
Cl5	Cl6	x, y, z	3.1644(12)
	Cl4	1-x, 1/2+y, 1/2-z	3.3294(14)
Cl6	Cl5	x, y, z	3.1651(12)
	Cl2	2-x, 1/2+y, 3/2-z	3.3461(14)